INSTITUTE OF PHYSICS PUBLISHING SMART MATERIALS AND STRUCTURES
Smart Mater. Struct. **14** (2005) 1297–1308 doi:10.1088/0964-1726/14/6/022

An enhanced SMA phenomenological model: I. The shortcomings of the existing models

Mohammad H Elahinia[1] **and Mehdi Ahmadian**[2]

[1] Department of Mechanical Industrial and Manufacturing Engineering, The University of Toledo, Toledo, OH 43606, USA
[2] Center for Vehicle Systems and Safety, Department of Mechanical Engineering, Virginia Tech, MC-0238 Blacksburg, VA 24061, USA

E-mail: mohammad.elahinia@utoledo.edu and ahmadian@vt.edu

Received 26 October 2004, in final form 14 July 2005
Published 17 October 2005
Online at stacks.iop.org/SMS/14/1297

Abstract
This paper provides an enhanced phenomenological model for shape memory alloys (SMAs), to better model their behavior in cases where the temperature and stress states change simultaneously. The phenomenological models for SMAs, consisting of a thermodynamics-based-constitutive and a phase transformation kinetics model, are the most widely used models for engineering applications. The existing phenomenological models are formulated to qualitatively predict the behavior of SMA systems for simple loadings. In this study, we have shown that there are certain situations in which these models are either not correctly formulated, and therefore are not able, to predict the behavior of SMA wires or the formulation is not straightforward for engineering applications. Such cases most often occur when the temperature and stress of the SMA wire change simultaneously, such as the case of rotary SMA actuators. To this end, a rotary SMA-actuated robotic arm is modeled using the existing constitutive models. The model is verified against the experimental results to document that the model is not able to predict the behavior of the SMA-actuated manipulator, under certain conditions.

1. Introduction

Shape memory alloys (SMAs) are a group of metal alloys that exhibit the characteristics of either large recoverable strains or large force due to temperature and/or load changes. The unique thermomechanical property of the SMAs is due to the phase transformation from the austenite (parent) phase to martensite (product) phase and vice versa. These transformations take place because of changes in the temperature, stress, or a combination of both. In the stress-free state, an SMA material at high temperature exists in the parent phase. The parent or austenite phase usually is a body centered cubic crystal structure. When the temperature of the material decreases the phase transforms into martensite which is usually a face centered cubic structure. In the stress-free state the martensite phase exists in multiple variants that are crystallographically similar but are oriented in different habit planes [1].

The observable macroscopic mechanical behavior of SMAs can be separated into two categories: the shape memory effect and pseudoelastic (superelastic) effect. In the shape memory effect, an SMA material exhibits a large residual strain after the loading and unloading. This strain can be fully recovered upon heating the material. In the pseudoelastic effect, the SMA material achieves a very large stain upon loading that is fully recovered in a hysteresis loop upon unloading [1]. SMAs show different mechanical behaviors at different temperatures. Some of the SMA stress–strain behaviors are illustrated in figure 1.

Since shape memory material behavior depends on stress and temperature and is intimately connected with the crystallographic phase of the material and the thermodynamics underlying the transformation process, the formulation of adequate macroscopic constitutive laws is necessarily complex [2]. There has been an extensive body of research

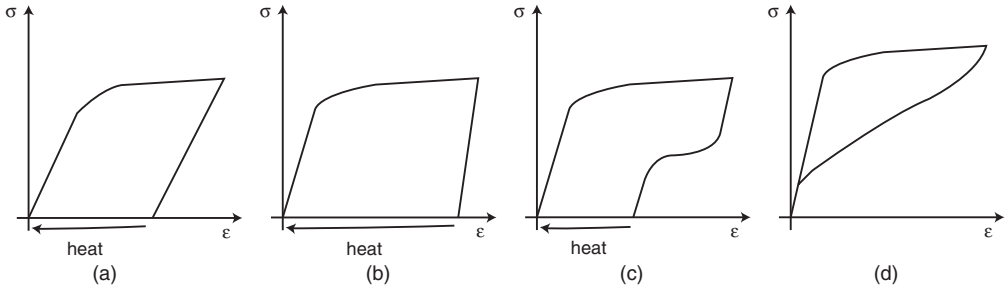

Figure 1. Mechanical behavior of a shape memory alloy. The nonlinear portion of the plot is due to detwinning the martensite variants or transforming the austenite to martensite. (a) $T < A_s$ at the beginning material is fully martensitic; (b) $M_s < T < A_s$ at the beginning material is fully austenitic; (c) $A_s < T < A_f$ at the beginning material is fully austenitic; (d) $T > A_f$ at the beginning material is fully austenitic [1].

on modeling the phase transformation and thermomechanical behavior of SMAs that is mostly devoted to one-dimensional SMA components. Brinson *et al* have divided these models into four categories [3]:

(1) models based on thermodynamics and derived from a free energy formulation [4–9],
(2) mathematical models for the dynamics of phase boundary motion [10–12],
(3) constitutive laws based on micromechanics concepts using energy dissipation guidelines [13, 14], and
(4) phenomenological laws based on uniaxial stress–strain–temperature data [15, 16, 1].

These constitutive models are each aimed at describing a different aspect of shape memory behavior and address the thermomechanical behavior of SMAs due to the phase transformation process on different scales.

Engineering applications have emphasized phenomenological models, which avoid difficult-to-measure parameters such as free energy and use only clearly defined engineering material constants. The focus of this part of the paper is on the adequacy of the phenomenological models for describing the behavior of the SMA elements under complex thermomechanical loads. This paper presents the shortcomings of the existing phenomenological models in predicting the behavior of SMA-actuated systems under complex thermomechanical loadings. The second part of the paper introduces an enhanced phenomenological model to address these shortcomings.

2. SMA phenomenological models

In 1986, Tanaka [17] presented a unified one-dimensional martensitic phase transformation model. His study was restricted to the stress-induced martensite phase transformation. The basic assumption was that the thermomechanical process of the material is fully described by three state variables: strain, temperature, and martensite fraction. The martensite fraction (ξ), as an internal variable, characterizes the extent of the martensite phase transformation. Choosing the Helmholtz free energy and using the Clausius–Duhem inequality, Tanaka developed the constitutive equation in the rate form, showing that the rate of stress is a function of the strain, temperature, and martensite fraction rates. If the expression for free energy is known, the free energy minimization may determine the equilibrium state and therefore the relation of the martensite fraction with applied stress and temperature. Instead, based on the study of the transformation kinetics, Tanaka assumed an exponential kinetics function.

The kinetics equation describes the phase transformation fraction as an exponential function of stress and temperature:

$$\begin{aligned} \xi_{M\to A} &= \exp[A_a(T - A_s) + B_a\sigma] \\ \xi_{A\to M} &= 1 - \exp[A_m(T - M_s) + B_m\sigma] \end{aligned} \tag{1}$$

where A_a, A_m, B_a, and B_m are material constants in terms of transition temperatures, A_s, A_f, M_s, and M_f. Tanaka qualitatively showed that the pseudoelasticity, ferroelasticity (partial pseudoelasticity), and shape memory effect can be described using a combination of the presented constitutive and kinetics models. The thermomechanical loadings that were considered are either isothermal mechanical loading or changing the temperature under stress-free conditions. An advantage of this model is that the parameters are simply determined by mechanical experiments.

Motivated by the need for a unified and theoretical constitutive model for SMA material, in 1990, Liang and Rogers developed a new phenomenological model based on the Tanaka model [18]. In their model Liang and Rogers adopted Tanaka's constitutive equation. For the phase kinetics, however, they assumed a cosine relationship to describe the martensite fraction as a function of the stress and temperature. Additionally, they assumed that the material properties are constant. The phase transformation kinetics equation for the heating is

$$\xi = \frac{\xi_M}{2}\cos[a_A(T - A_s) + b_A\sigma] + \frac{\xi_M}{2}. \tag{2}$$

The phase transformation equation for the cooling is

$$\xi = \frac{1 - \xi_A}{2}\cos[a_M(T - M_f) + b_M\sigma] + \frac{1 + \xi_A}{2} \tag{3}$$

where $a_A = \frac{\pi}{A_f - A_s}$, $a_M = \frac{\pi}{M_s - M_f}$ are two material constants, and A_f, A_s, M_f, and M_s are austenite final, austenite start, martensite final and martensite start temperatures, respectively. The two other material constants are defined as $b_A = -\frac{a_A}{C_A}$ and $b_M = -\frac{a_M}{C_M}$. C_A and C_M indicate the influence of stress on these four transformation temperatures. Furthermore, ξ_M

and ξ_A are the martensite fraction reached before heating and cooling, respectively.

The argument for the cosine functions should be between 0 and π, which means that the transformation takes place only if the temperature is in the transformation range:

$$A_s \leqslant T \leqslant A_f \qquad \text{or} \qquad M_f \leqslant T \leqslant M_s. \tag{4}$$

Equivalently, the stress range for the martensite to austenite phase transformation is defined as

$$C_A(T - A_s) - \frac{\pi}{|b_A|} \leqslant \sigma \leqslant C_A(T - A_s) \tag{5}$$

and the corresponding stress range for the austenite to martensite transformation is defined as

$$C_M(T - M_f) - \frac{\pi}{|b_M|} \leqslant \sigma \leqslant C_M(T - M_f). \tag{6}$$

In 1993, Brinson [1] developed a one-dimensional model for SMAs based on the previous works of Tanaka and Liang. The same constitutive equation that was initially introduced by Tanaka was adopted considering the same thermodynamics principles. For the phase transformation kinetics, however, Brinson used Liang's model rewritten as

$$\xi = \frac{\xi_0}{2}\cos\left[a_A\left(T - A_s - \frac{\sigma}{C_A}\right)\right] + \frac{\xi_0}{2}. \tag{7}$$

for $C_A(T - A_f) < \sigma < C_A(T - A_s)$, and

$$\xi = \frac{1 - \xi_0}{2}\cos\left[a_M\left(T - M_f - \frac{\sigma}{C_M}\right)\right] + \frac{1 + \xi_0}{2} \tag{8}$$

for $C_M(T - M_s) < \sigma < C_M(T - M_f)$. Although it is not stated by Brinson, one can assume that equation (7) is for heating (martensite to austenite transformation) and equation (8) is for cooling (austenite to martensite transformation). C_A and C_M are defined as material properties defining the relationship between temperature and the critical stresses that induce the transformation.

The Brinson model does not have one of the shortcomings of Liang model. The Liang model cannot describe the shape memory effect, which takes place because of detwinning of the martensite, at temperatures below M_f. Brinson separated the martensite fraction into two fractions as the fraction induced by stress and the fraction induced by temperature:

$$\xi = \xi_s + \xi_T. \tag{9}$$

The constitutive equation was also modified accordingly:

$$\dot{\sigma} = D\dot{\varepsilon} + \Theta\dot{T} + \Omega\dot{\xi}_s. \tag{10}$$

The phase transformation equations are similar to the ones presented by Liang written in terms of critical stresses. Therefore, the Brinson model is capable of the showing shape memory effect at lower temperature which takes place as the result of detwinning, not as the result of the austenite to martensite phase transformation. Furthermore, in the Brinson model the elastic modulus and the transformation tensor were assumed to be functions of the martensite fraction.

Brinson and Bekker developed a set of phase kinetics laws for the austenite to detwinned martensite and martensite to austenite phase transformations [19, 20]. These phase transformation models predict the martensite fraction as a function of the loading path Ł, initial state of the material ξ_0, stress σ, and temperature T at time t.

$$\xi(t) = \Phi(T(t), \sigma(t); \xi_0)_{(T,\sigma)\in Ł} \tag{11}$$

where

$$\Phi(T(t), \sigma(t); \xi_0) = \begin{cases} F^A(T, \sigma; T_0, \sigma_0; \xi_0), \\ \qquad \text{if } Ł \in [A] \text{ and } Ł \uparrow\uparrow \mathbf{n}^A \\ F^M(T, \sigma; T_0, \sigma_0; \xi_0), \\ \qquad \text{if } Ł \in [M] \text{ and } Ł \uparrow\uparrow \mathbf{n}^M \\ F^D = \xi_0, \\ \qquad \text{otherwise.} \end{cases} \tag{12}$$

The functions F^A, F^M, and F^D are branches of the phase kinetic law, $\mathbf{n}$ is the normal vector to the phase transformation strip. According to equation (12), the martensite to austenite phase transformation takes place if the loading path Ł and the normal vector to the austenite start temperature line have a component in the same direction ($Ł \uparrow\uparrow \mathbf{n}^A$).

3. SMA-actuated robotic arm

In order to further investigate the SMA phenomenological models, an SMA-actuated robotic arm is studied in this section. Using the existing phenomenological models, the system is modeled, the derived model is simulated, and the simulation results are compared with experimental data. The shortcomings of the SMA models in predicting the complete behavior of the SMA-actuated arm are studied using the simulation results of the system. Using a dead-weight system that is actuated by an SMA wire, the model shortcomings are experimentally studied, in part II. An enhanced model is developed to address the shortcomings of the existing SMA phenomenological models. Furthermore, based on the enhanced phenomenological model, a general procedure for modeling systems that are actuated by shape memory alloys is presented.

The one-degree-of-freedom shape memory alloy (SMA) actuated arm is shown in figure 2. The shape memory effect (SME) is not reversible; the SMA wire must be deformed by a bias force in martensite to repeat the movement. There are two ways of providing the bias force and therefore two types of SMA actuator. One actuator, called *bias type*, is composed of an SMA element and a bias spring. The other, called *differential type*, is made of two SMA elements. In our design the robotic arm is actuated with a bias-type SMA wire actuator where the bias force (torque) is provided by the linear spring and the weight of the moving arm. Therefore, the generating torque is the difference between the bias torque and SMA wire torque.

When the SMA wire is heated beyond the activation temperature it contracts due to the phase transformation from martensite to austenite. The temperature is raised using the resistive electrical (Joule) heating. Upon cooling, the wire's temperature drops, causing the austenite to martensite phase transformation. As a result the SMA wire is elongated under the effect of the bias torque. While elongating, the twinned

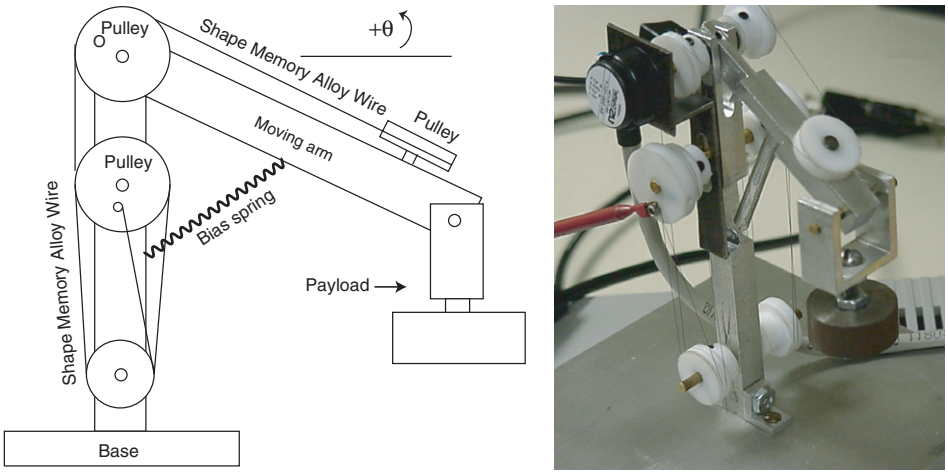

Figure 2. The one-degree-of-freedom arm, actuated by SMA NiTi wire, with a bias spring.
(This figure is in colour only in the electronic version)

martensite changes to the stress-preferred martensite. The initial length of the SMA wire, that is guided by the pulleys, is chosen in a way that upon full contraction it can rotate the arm from its initial position at −45° to the top position at +90°.

The model for the SMA-actuated arm consists of phase transformation kinetics, heat transfer, SMA wire constitutive, and arm dynamic model blocks. The input is voltage (to the SMA wire applied through an amplifier) and the outputs are the arm angular position, arm angular velocity, the SMA wire's temperature, stress, and the martensite fraction.

4. Heat transfer model

The SMA wire heat transfer equation consists of electrical (Joule) heating and natural convection:

$$mc_p \frac{\mathrm{d}T}{\mathrm{d}t} = I^2 R - h_\mathrm{c} A_\mathrm{c}(T - T_\infty). \tag{13}$$

The SMA wire that is used in the system is Ni–Ti alloy. Its diameter is 150 μm and the parameters in the heat transfer equation are: $m = (\rho\pi\frac{d^2}{4})$ is mass per unit length of wire, ρ is density of wire, d is diameter of wire, $A_\mathrm{c} = (\pi d)$ is circumferential area of the unit length of wire, c_p is specific heat, I is electrical current, R is resistance per unit length of wire, T is temperature of wire, T_∞ is the ambient temperature, and h_c is the heat convection coefficient. Although here we assumed that the h_c and R are both constant, a detailed analysis on heat transfer as well as resistance analysis of the SMA wire can be found in the appendix.

5. Wire constitutive model

The wire constitutive model shows the relationship between stress, strain and temperature. We used the phenomenological model presented by Tanaka [17] and later completed by Liang [18] and Brinson [1]. The basic equation is

$$\dot{\sigma} = E\dot{\varepsilon} + \theta_\mathrm{T}\dot{T} + \Omega\dot{\xi} \tag{14}$$

where E is the Young's modulus, θ_T is the thermal expansion factor, $\Omega = -E\overline{\varepsilon_L}$ is the phase transformation contribution factor, and $\overline{\varepsilon_L}$ is the maximum recoverable strain.

6. Phase transformation model

For simulating the constitutive equation, the value of the martensite fraction derivative needs to be known at each instant of time. Based on the hysteresis behavior of SMA wires, a cosine phase kinetics model is developed by Liang [16]. The phase kinetics model needs temperature and stress to calculate the fraction. Due to the hysteresis behavior of SMA wires the equations for heating and cooling are different.

7. Reverse transformation

The reverse transformation equation describing the phase transformation from martensite to austenite (heating) is

$$\xi = \frac{\xi_\mathrm{M}}{2}\{\cos[a_\mathrm{A}(T - A_s) + b_\mathrm{A}\sigma] + 1\} \tag{15}$$

where ξ is martensite fraction, which has a value between 1 (martensite phase) and 0 (austenite phase). ξ_M is the minimum martensite fraction the wire reached during the cooling. $a_\mathrm{A} = \frac{\pi}{A_\mathrm{f} - A_\mathrm{s}}(^\circ\mathrm{C}^{-1})$ is a curve-fitting parameter, T is the wire's temperature, σ is the wire's stress, A_s is the austenite phase start temperature, A_f is the austenite phase final temperature, and $b_\mathrm{A} = \frac{-a_\mathrm{A}}{C_\mathrm{A}}$ and C_A are curve-fitting parameters.

Therefore, the derivative equation for heating can be written as

$$\dot{\xi} = \frac{-\xi_\mathrm{M}}{2}\sin[a_\mathrm{A}(T - A_\mathrm{s}) + b_\mathrm{A}\sigma][a_\mathrm{A}\dot{T} + b_\mathrm{A}\dot{\sigma}]. \tag{16}$$

If $A'_\mathrm{s} = (A_\mathrm{s} + \frac{\sigma}{C_\mathrm{A}}) < T < (A_\mathrm{f} + \frac{\sigma}{C_\mathrm{A}}) = A'_\mathrm{f}$.

Otherwise $\dot{\xi} = 0$. Here A'_s and A'_f are the *stress modified* austenite start and final temperatures, respectively.

8. Forward transformation

The forward transformation equation describing the phase transformation from austenite to martensite (cooling) is

$$\xi = \frac{1 - \xi_\mathrm{A}}{2}\cos[a_\mathrm{M}(T - M_\mathrm{f}) + b_\mathrm{M}\sigma] + \frac{1 + \xi_\mathrm{A}}{2} \tag{17}$$

Table 1. Modeling parameters and their numerical value.

Parameter	Description	Unit	Value
m	SMA wire's mass per unit length	kg	1.14×10^{-4}
A_c	SMA wire's circumferential area per unit length	m^2	4.712×10^{-4}
C_p	Specific heat of wire	kcal kg^{-1} °C^{-1}	0.2
R	SMA wire's resistance per unit length	Ω	45
T_∞	Ambient temperature	°C	20
h_c	Heat convection coefficient	J m^{-2} °C^{-1} s^{-1}	150
E_A	Austenite Young modulus	GPa	75.0
E_M	Martensite Young modulus	GPa	28.0
θ_T	SMA wire's thermal expansion factor	MPa °C^{-1}	0.55
Ω	Phase transformation contribution factor	GPa	−1.12
σ_0	SMA wire's initial stress	MPa	75.0
ε_0	SMA wire's initial strain		0.04
T_0	SMA wire's initial temperature	°C	20
ξ_0	SMA wire's initial martensite faction factor		1.0
A_s	Austenite start temperature	°C	68
A_f	Austenite final temperature	°C	78
M_s	Martensite start temperature	°C	52
M_f	Martensite final temperature	°C	42
C_A	Effect of stress on austenite temperatures	MPa °C^{-1}	10.3
C_M	Effect of stress on martensite temperatures	MPa °C^{-1}	10.3
l_0	Initial length of SMA wire	mm	900
r	Pulleys diameter	mm	8.25
m_p	Pay load mass	g	57.19
m_a	Moving link mass	g	18.7
k	Bias spring stiffness	N m^{-1}	3.871

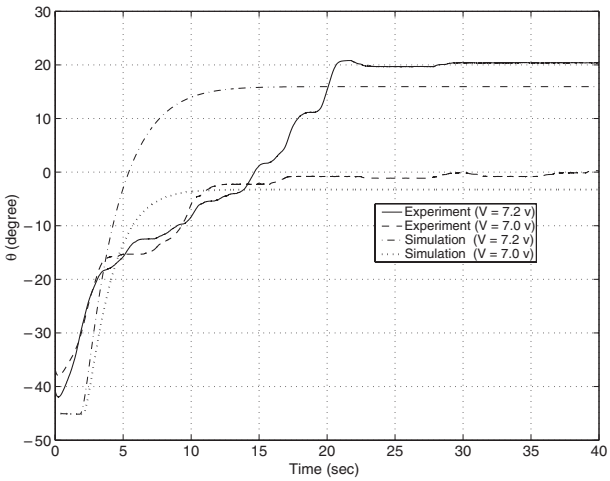

Figure 3. Comparison of theoretical model simulations and experimental results.

where ξ_A here is the minimum martensite fraction obtained during heating, $a_M = \frac{\pi}{M_s - M_f}$ is a curve-fitting parameter, M_s is the martensite phase start temperature, M_f is the martensite phase final temperature, and $b_M = \frac{-a_M}{C_M}$ is a curve-fitting parameter.

Therefore, the derivative equation for cooling can be written as

$$\dot{\xi} = \frac{1 - \xi_A}{2}\{-\sin[a_M(T - M_f) + b_M\sigma]\}[a_M\dot{T} + b_M\dot{\sigma}]. \quad (18)$$

If $M'_f = (M_f + \frac{\sigma}{C_M}) < T < (M_s + \frac{\sigma}{C_M}) = M'_s$.

Otherwise $\dot{\xi} = 0$. Here M'_s and M'_f are the *stress modified* martensite start and final temperatures, respectively.

9. Kinematic model

The kinematic model describes the relationship between strain ε and angular displacement θ. Measuring positive angle clockwise, the equation is

$$\dot{\varepsilon} = -\frac{2r\dot{\theta}}{l_0} \quad (19)$$

where r is the pulley's radius and l_0 is the wire's initial length.

10. Dynamic model

The nonlinear dynamic model of the arm including spring and payload effects is

$$I_e\ddot{\theta} + \tau_g + \tau_s + c\dot{\theta} = \tau_w \quad (20)$$

where τ_w, τ_g, and τ_s are the resulting torques from the SMA wire, gravitational loads, and spring, respectively. I_e is the effective mass moment of inertia of the arm, and the payload, and c is the torsional damping coefficient.

11. Model simulation and verification

The material properties of the shape memory alloy are primarily taken from Liang [16] and Waram [21], which are shown in table 1. Experimental evaluations, by Elahinia and Ashrafiuon [22], have demonstrated reasonable accuracy of the actuator model, as is shown in figure 3. The figure compares simulation and experimental results at 7.0 and 7.2 V. Some of the differences between the simulation and experimental results are due to parameter uncertainties and model simplifications. Specifically, the modulus,

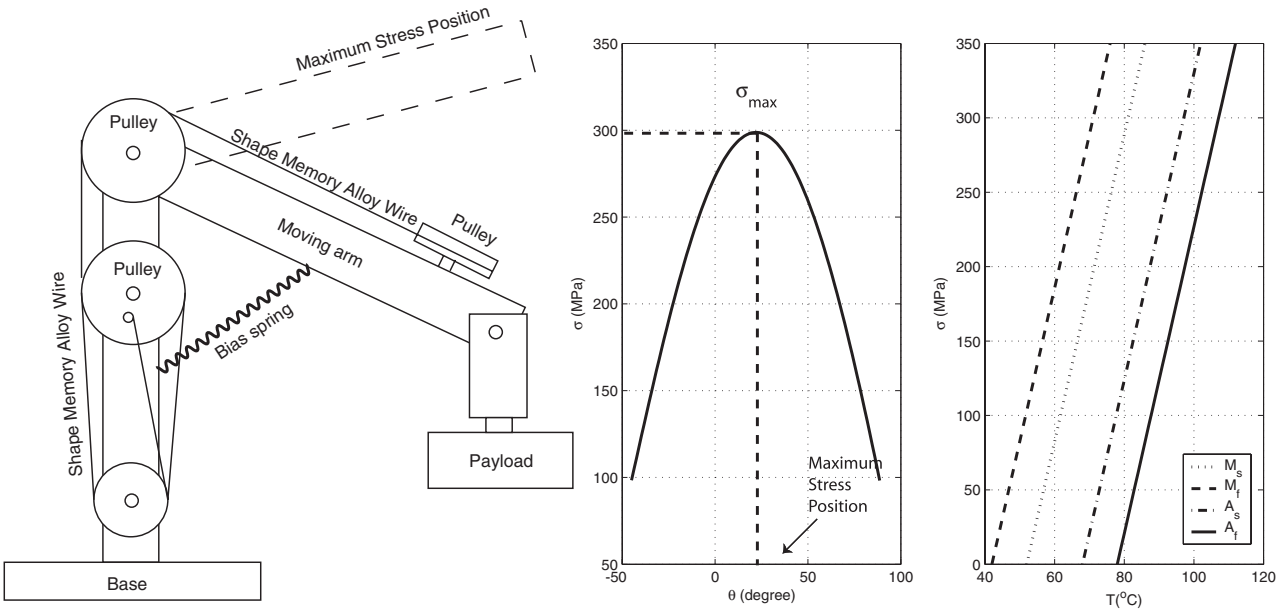

Figure 4. When the arm moves beyond the maximum stress position the transformation temperatures decrease.

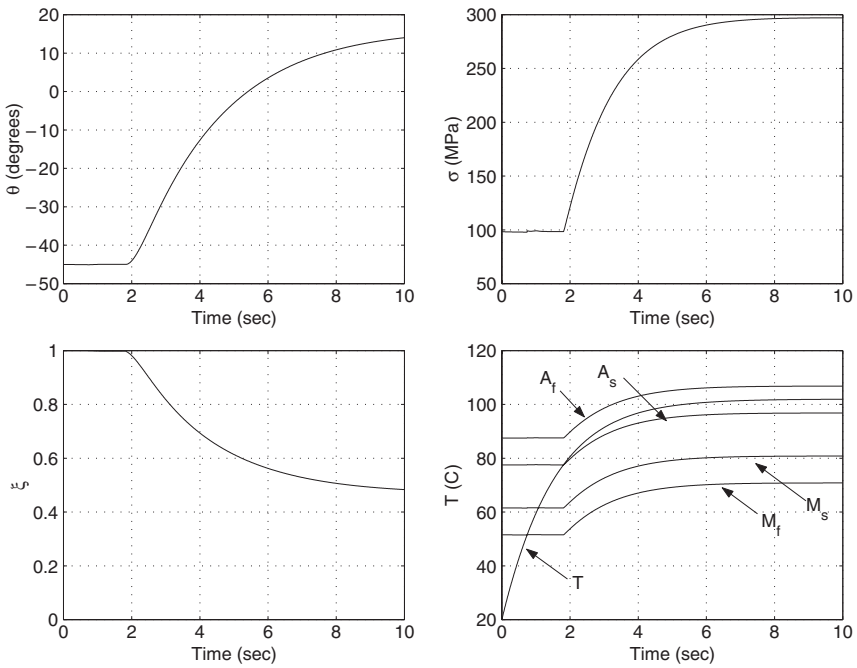

Figure 5. SMA model open-loop simulation for a 7.2 V input.

transformational tensor, and thermal coefficient were all assumed to be constant. The assumptions of a linear spring force and viscous friction contributed to the discrepancy of the results.

The main qualitative aspects of the SMA arm model can be derived from figures 5 and 6. In figure 5, a 7.2 V input is applied to the actuator and the temperature of the wire rises. The initial martensite fraction is equal to 1 and no phase transformation takes place as the temperature increases past the martensite final temperature, M_f. As the wire continues to heat, the temperature exceeds the austenite start temperature, A_s, and the martensite fraction decreases—resulting in contraction of the wire—at a rate defined by the derivative of equation (16). In steady state, the temperature falls somewhere between the austenite start and final temperatures, hence only partial transformation is achieved.

As is shown in figure 6, only a slightly larger voltage, 7.3 V, results in a full transformation to austenite. The increased voltage heats the wire enough to cause the arm to rotate through the angle of maximum stress. At this angle, shown in figure 4,

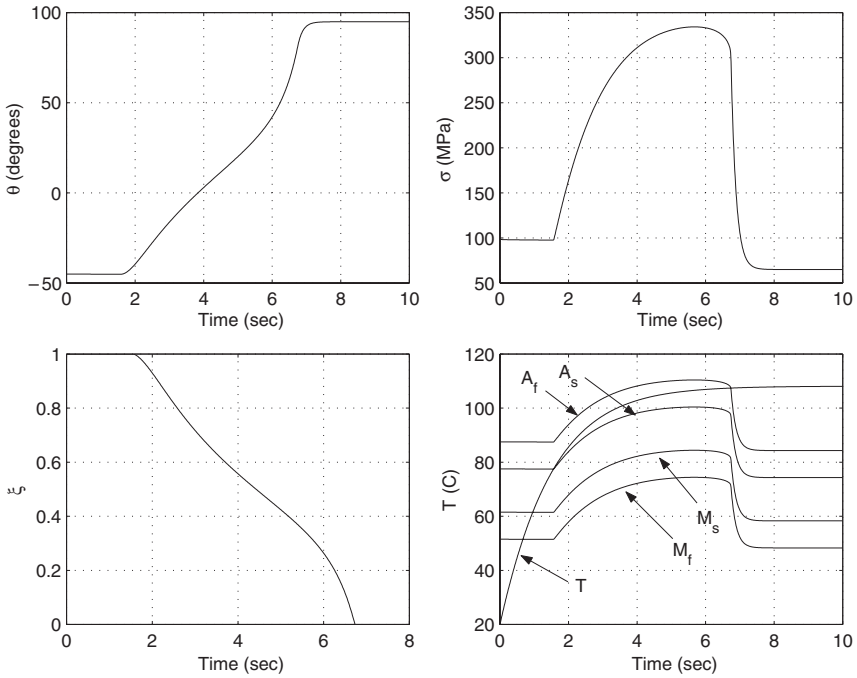

Figure 6. SMA model open-loop simulation for a 7.3 V input.

the stress of the SMA wire due to gravitational and spring torques is maximum. Upon passing this angle, the stress in the wire begins to decrease rapidly, which results in a drop in the transformation temperatures. This drop allows the temperature of the wire to pass through the austenite final temperature, causing the martensite fraction to fall to zero and the wire to achieve maximum strain.

12. SMA phenomenological models: where they fail

While the SMA phenomenological models give proper results for most cases, there are certain complex loading cases in which the output of these models does not match experimental results. An example of this shortcoming is presented in this section. The phase transformation kinetics by Liang [18] and Brinson [1] are adopted in this study. Since in the rotary SMA actuator the wire is always under stress, by the bias spring, these two phenomenological models predict similar behaviors. It is worth noting that the Brinson and Bekker phase model covers the general loading conditions and their corresponding phase transformations and therefore does differentiate between the cases shown in figure 11. This phase transformation model, however, is not easy to implement for engineering applications since it requires finding and updating several points along the loading path. An easy-to-use phase transformation kinetics formulation is therefore needed to use in conjunction with the phase transformation models for numerical simulation of the SMA-actuated systems that undergo complex thermomechanical loadings. To address this need a phase transformation model is developed as presented in the next section.

Figure 7 shows an example of the shortcomings of these models. In this simulation, a sliding mode controller was used to stabilize the rotary SMA actuator (for details see [23]). As shown in the figure, the controller was not able to regulate the arm at $\theta_d = 85°$. As figure 8 shows, the controller applied high enough voltage such that the temperature of the wire exceeded the austenite final temperature, in an attempt to minimize the position error. Even though the temperature of the wire reached beyond the austenite final temperature, according to the model, the wire did not go through the full phase transformation, as shown in figure 9. Therefore the arm did not reach the desired angular position. Such a behavior has never been observed in the experiments with the SMA-actuated arm; in other words it has never been observed that the voltage to the SMA wire was increased but the arm did not move accordingly unless the SMA wire was already in the fully austenitic phase. Furthermore, according to the aforementioned phenomenological models, if the temperature of the SMA wire exceeds the austenite final temperature the material reaches the fully austenitic phase ($\xi = 0$), which clearly has not happened in this example.

Figure 10 illustrates why in this and similar cases the existing phenomenological models cannot predict the behavior of SMA wire: in the simulation, the temperature of the SMA wire exceeded the austenite final temperature while the temperature itself was decreasing. While the SMA wire was cooling down, the stress of the wire decreased, which caused the austenite final temperature to decrease. The rates of temperature decrease for the wire and the austenite final temperature are not equal: the SMA wire's temperature decays slower than the austenite final temperature; this way the wire's temperature—while decreasing—exceeded the austenite final temperature. According to the existing phenomenological models, no phase transformation takes place between the austenite start and final temperatures unless the temperature is increasing.

Similar cases exist in which the existing phenomenological models cannot predict the behavior of SMA wires. Three

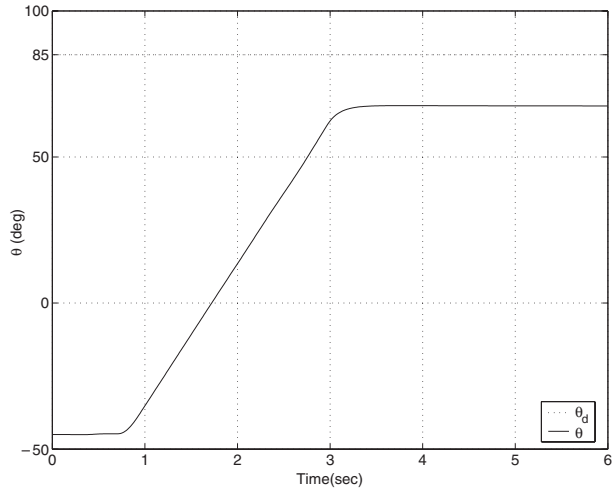

Figure 7. Phase transformation model problem: arm does not reach the desired position.

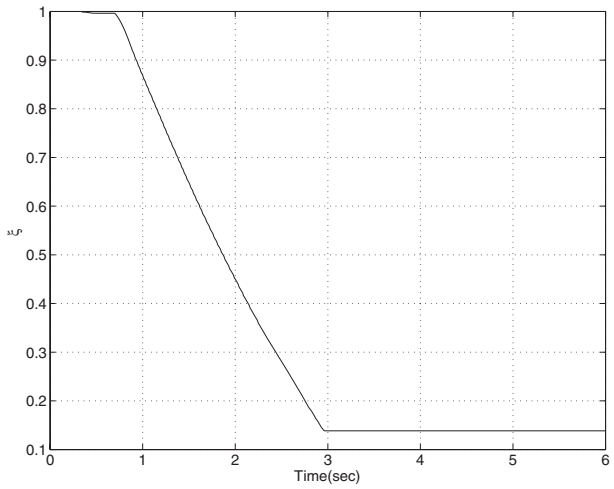

Figure 9. Phase transformation model problem: martensite fraction.

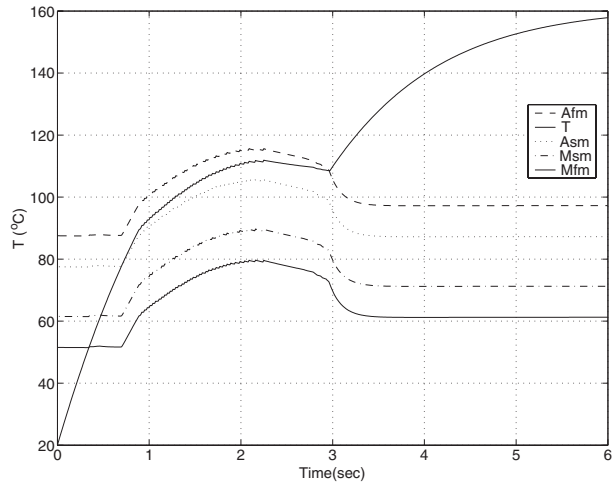

Figure 8. Phase transformation model problem: temperature of the SMA wire and transformation temperatures.

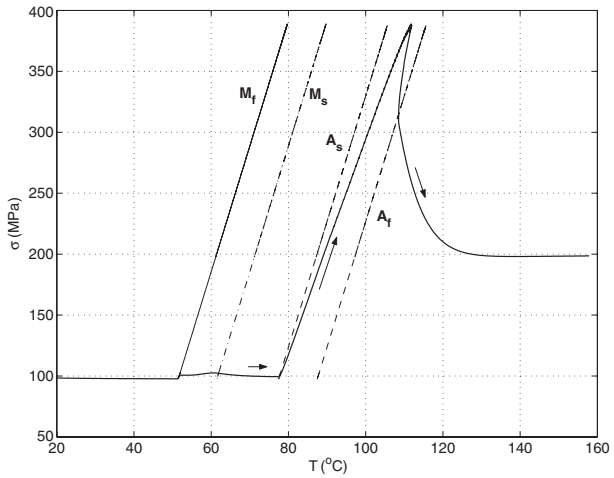

Figure 10. Phase transformation model problem: stress versus temperature.

such cases are illustrated in figure 11. For all the cases shown in the figure, according to these models, the amount of phase transformation that takes place is the same. In all three cases, the stress of the wire decreases by the same amount, which consequently causes the austenite start and final temperatures to drop. This effect is shown in the figure as similar shifts in the hysteresis loop in the $(T$–$\xi)$ plane. In figure 11(a) the wire cools down but with a slower rate, and therefore the temperature exceeds the austenite final temperature. The example with the SMA-actuated robotic arm, as illustrated in figure 10, in which the arm did not reach the desired position, falls in this category. In figure 11(b) the wire cools down such that the temperature remains between the austenite start and final. In the third case, as shown in figure 11(c), the temperature remains constant and still exceeds the austenite final temperature. For all these three cases with similar stress changes but dramatically different temperature changes the existing phenomenological models predict the same martensite fraction at point 2. In other words, no further phase transformation takes place beyond point 1.

Figures 12–15 depict the same simulation results for a simulation with SMA-actuated robotic arm. In this case the arm was to track a changing step. Since the SMA wire did not undergo any of the complex loading patterns, the existing phase transformation models calculated the martensite fraction properly.

13. Summary

The existing SMA phenomenological models were investigated, using an SMA-actuated robotic arm. The model was verified against experimental data. Using simulations, it was shown that for cases that involve complex thermomechanical loadings—in terms of simultaneous changes in stress and temperature—the existing phenomenological models have shortcomings. In a following paper, these shortcomings will be further highlighted using the experimental data with a dead-weight SMA actuator. Finally, an enhanced phenomenological model will be presented. This mode is able to predict

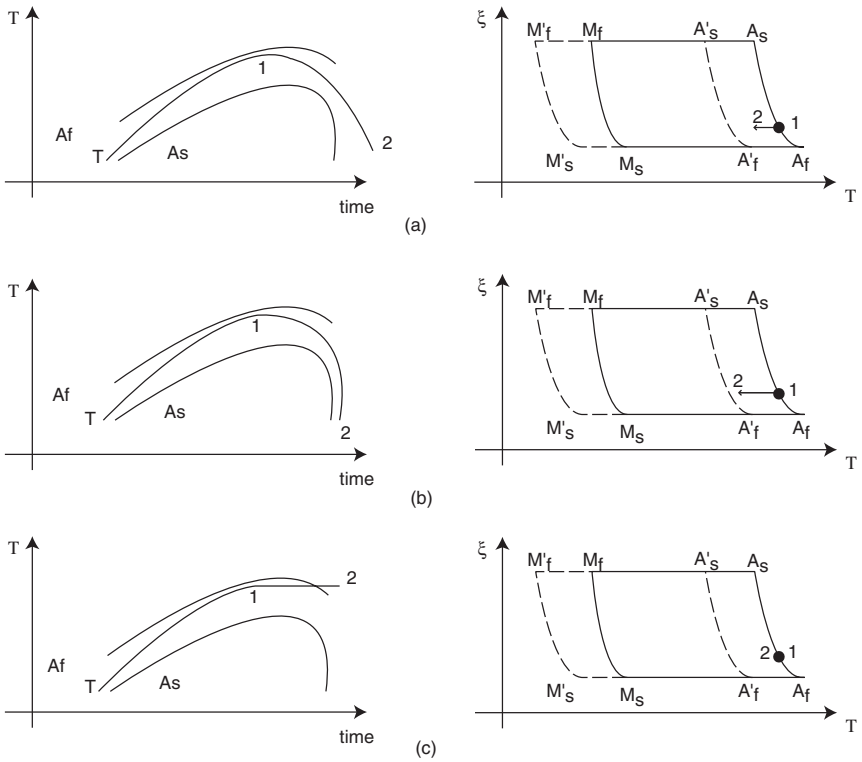

Figure 11. The shortcomings of the phase transformation model in predicting the martensite fraction for complex force and heat loading, (a) exceeding the austenite final temperature while cooling; (b) remaining in the phase transformation range while cooling; (c) exceeding austenite final temperature with constant temperature.

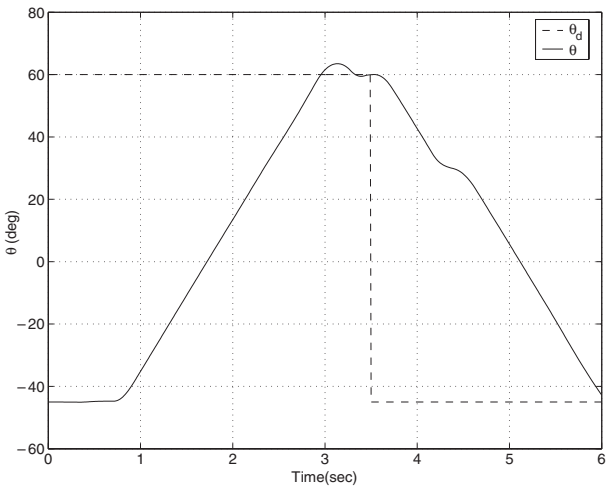

Figure 12. Phase transformation model works properly: arm follows the desired position.

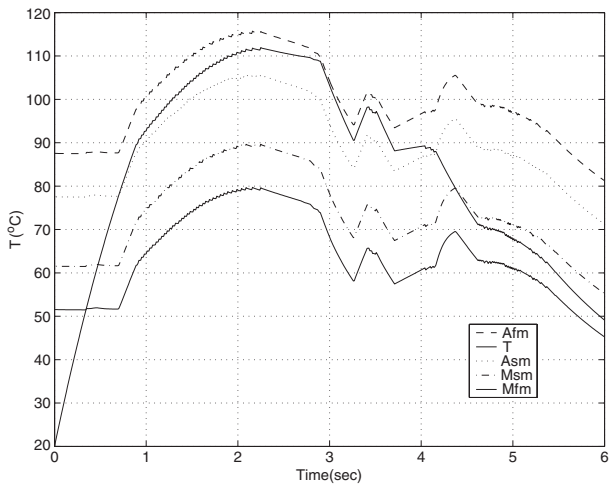

Figure 13. Phase transformation model works properly: temperature of the SMA wire and transformation temperatures.

the behavior of SMA wires under complex thermomechanical loadings.

Appendix

A.1. Heat transfer analysis

There are number of studies on the heat transfer of the SMA materials. A representative example is the work of Bhattacharyya *et al* [24] in which they studied the possibility of using the thermoelectric effect in order to improve the cooling response of the SMA actuators. Bhattacharyya *et al* [25] also worked on the characterization of the convection heat transfer coefficient for SMA wires. They modeled the coefficient as a linear function of the current of the wire and performed experiments with SMA and non-SMA wires to verify the model. Potapov and da Silva [26] used Liang's kinematics model for SMA elements with constant stress and constant

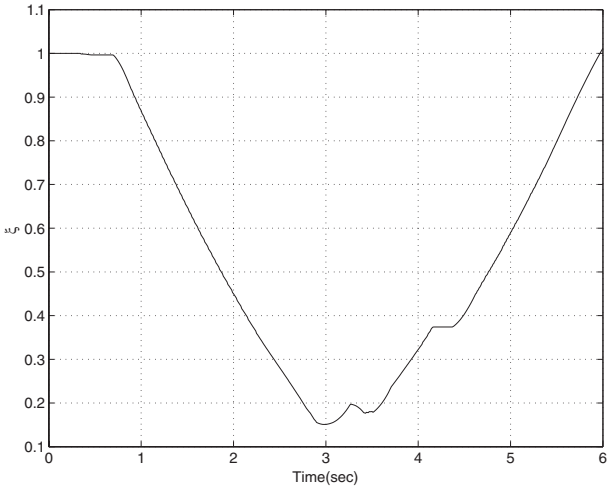

Figure 14. Phase transformation model works properly: martensite fraction.

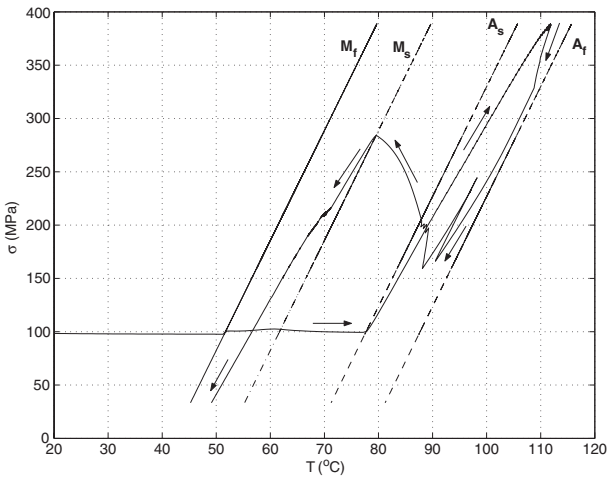

Figure 15. Phase transformation model works properly: stress versus temperature.

strain in order to find both heating and cooling response times. They assumed the convection heat transfer to be constant and showed that the time constant is in agreement with the experiments.

Here we have used the principle of the conservation of energy to model the heat transfer behavior of the SMA wire. Unlike the works of Bhattacharyya *et al* [25] and Potapov and da Silva [26] we have used a convection heat transfer coefficient that is based on the thin cylinder theory. As explained next, the convection coefficient is found to be a function of wire temperature.

The heat transfer model of the wire, using the principle of conservation of energy, is written as

$$mC_p\frac{\mathrm{d}T}{\mathrm{d}t} = I^2R(\xi) - h(T)A(T - T_\infty) - m\Delta H\dot{\xi} \qquad (21)$$

where C_p is the specific heat, I and R are electric current and resistance, respectively, $h(T)$ is the convection heat transfer, A is the circumference area of the wire, T and T_∞ are the temperature of the wire and ambient, respectively, and ΔH is the latent heat associated with the phase transformation [26]. This equation presents the effect of the Joule heating, convection heat transfer, and latent heat on the internal energy of the wire.

A.2. Convection heat transfer

Natural heat convection takes place because of buoyancy force and the difference between cold and warm air densities. Because of the temperature difference between the vertical surfaces, in this case a cylindrical surface, and the ambient a boundary layer flow develops over the lateral surface. When the boundary layer thickness is smaller than the cylinder diameter, the cylinder can be modeled as a vertical wall, ignoring its curvature. In the case of a thin wire, however, the diameter is not necessarily larger than the boundary layer thickness and hence a different Nusselt number and therefore a different convection coefficient should be used. The criterion for considering a cylinder as a vertical wall is

$$\frac{D}{l} > Ra_l^{-\frac{1}{4}} \qquad (22)$$

where D and l are the cylinder's diameter and length, respectively, and Ra_l is the Rayleigh number. It can be shown that for the SMA wire this condition is not satisfied for the range of temperature of interest. On the other hand for vertical thin cylinders the Nusselt number is written as

$$\overline{Nu}_l = \frac{4}{3}\left[\frac{7Ra_l Pr}{5(20+21Pr)}\right]^{\frac{1}{4}} + \frac{4(272+315Pr)l}{35(64+63Pr)D} \qquad (23)$$

where Pr is the Prandtl number, $\overline{Nu}_l = hl/k$, and $Ra_l = g\beta\Delta Tl^3/\alpha\nu$. In these definitions h is the length-averaged heat transfer coefficient, and ΔT is the temperature difference between the surface of the ambient. Also β is the volume expansion coefficient that for the ideal gas can be shown to be $\beta = \frac{1}{T}$, where T is the absolute temperature. k, α and ν are thermal conductivity, thermal diffusivity and kinematic viscosity of the air calculated at the film temperature $T_\mathrm{f} = \frac{T+T_\infty}{2}$.

Therefore the convection coefficient is a function of both the temperature of the wire and the ambient temperature. We assume that the ambient temperature is constant while the wire's temperature changes considerably. Table A.1 shows the property of the air over the actuation temperature range [27]. The ambient temperature is assumed to be 23 °C. Using these properties the convection coefficient can be calculated. Figure A.1 shows the calculated convection heat transfer coefficient which increases as a function of the temperature of the wire. As shown in the figure, we have approximated it with a linear function as $h(T) = 0.1558T + 89.33$, where T is the temperature of the wire in centigrade.

It is worth noting that the cooling rate is proportional to the ratio of the surface area to the heat capacity. Thus the ratio of the surface area to the volume of the wire is a indicator of the cooling rate. The generating force on the other hand is proportional to the sectional area of the wire. The surface area/volume is in inverse proportion to the diameter. Therefore, if the diameter is small, the cooling rate is fast. However, the generating force is much smaller.

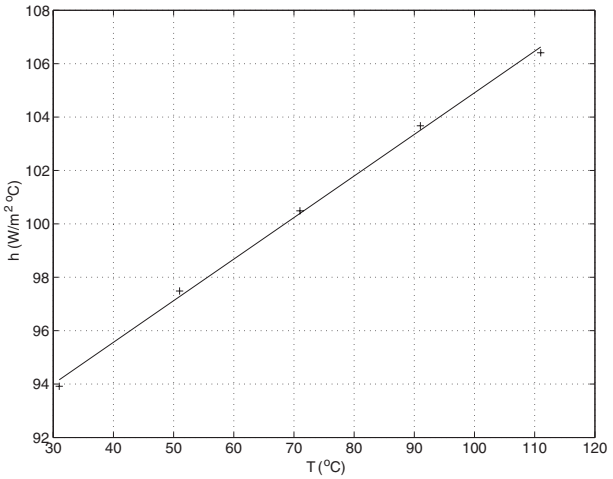

Figure A.1. The convection heat transfer coefficient as a function of the SMA wire temperature.

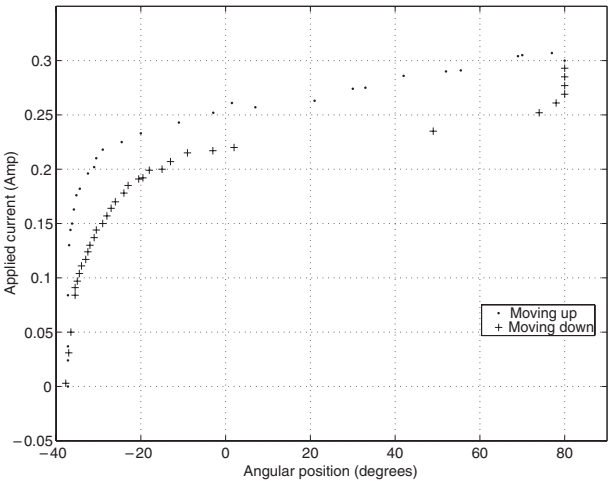

Figure A.2. The current passing through the SMA wire changes as a hysteretic function of the angular position of the actuator.

Table A.1. Air properties as a function of the SMA wire temperature; the ambient temperature is assumed to be $T_\infty = 23\,^\circ\mathrm{C}$).

T_w (°C)	T_f (K)	k (W m^{-1} °C^{-1})	α (m^2 s^{-1})	ν (m^2 s^{-1})	Pr
31	300	0.0261	2.21×10^{-5}	1.57×10^{-5}	0.712
51	310	0.0268	2.35×10^{-5}	1.67×10^{-5}	0.711
71	320	0.0275	2.49×10^{-5}	1.77×10^{-5}	0.710
91	330	0.0283	2.64×10^{-5}	1.86×10^{-5}	0.708
111	340	0.0290	2.78×10^{-5}	1.96×10^{-5}	0.707

A.3. Using SMA for sensing

Although SMAs are mostly used for actuation they also have a good sensing capability. Several properties of an SMA element change as it undergoes martensite phase transformation. Among these properties is the resistivity of SMAs that decreases as the temperature of the wire increases and hence its phase transforms to austenite. Using the SMA rotary actuator we conducted an experiment to evaluate the change in the resistance of the SMA wire.

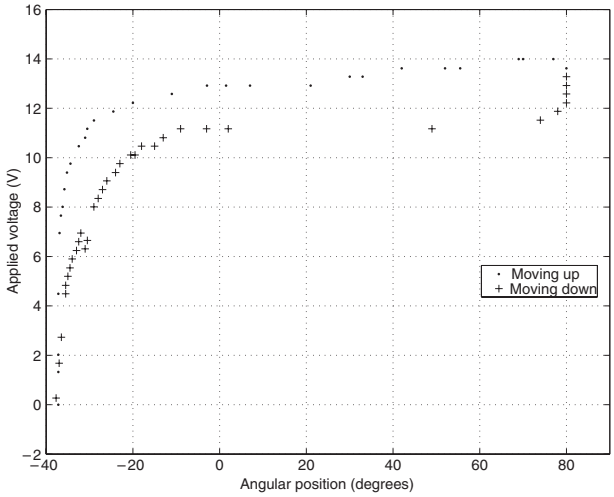

Figure A.3. The voltage of the SMA wire changes as a hysteretic function of the angular position of the actuator.

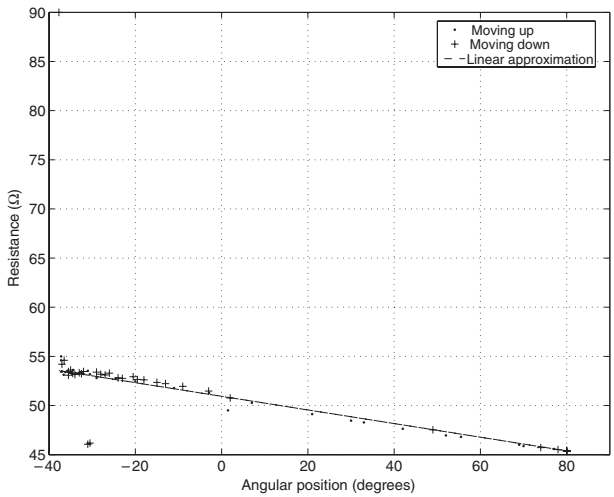

Figure A.4. The resistance of the SMA wire changes almost as a linear function of the angular position of the actuator.

In the experiment the applied voltage to the wire increased incrementally while recording the current and angular position of the moving arm. Phaser transformation is hysteretic, therefore the voltage, current and angular position were also recorded while the arm moved down due to the voltage drop. Figures A.2 and A.3 show the hysteretic plot of the voltage and current versus angular position of the actuator.

While the voltage and current both change with angular position in a hysteretic fashion the resistance of the wire changes almost linearly with the angle. This is shown in figure A.4 along with the linear approximation of resistance as a function of the angular position. The resistance is approximated as

$$R = -2.914\theta + 50.94. \tag{24}$$

This experiment is an indication of sensing capabilities of the SMA elements that can be further utilized.

References

[1] Brinson L C 1993 One-dimensional constitutive behavior of shape memory alloys: thermomechanical derivation with non-constant material functions and redefined martensite internal variable *J. Intell. Mater. Syst. Struct.* **4** 229–42

[2] Brinson L C and Huang M S 1996 Simplifications and comparisons of shape memory alloy constitutive models *J. Intell. Mater. Syst. Struct.* **7** 108–14

[3] Brinson A, Bekker L C and Hwang S 1996 Deformation of shape memory alloy due to thermo-induced transformation *J. Intell. Mater. Syst. Struct.* **7** 97–107

[4] Falk F 1980 Model free energy, mechanics, and thermodynamics of shape memory alloys *Acta Metall.* **28** 1773–80

[5] Maugin G A and Cadet S 1991 Existence of solitary waves in martensitic alloys *Int. J. Eng. Sci.* **29** 243–58

[6] Ivshin Y and Pence T J 1994 A thermomechanical model for a one variant shape memory alloy *J. Intell. Mater. Syst. Struct.* **5** 455–73

[7] Boyd J G and Lagoudas D C 1996 A thermodynamical constitutive model for shape memory materials. part I the monolithic shape memory alloy *Int. J. Plast.* **12** 805–42

[8] Boyd J G and Lagoudas D C 1996 A thermodynamical constitutive model for shape memory materials. Part I the SMA composite material *Int. J. Plast.* **12** 843–73

[9] Panoskaltsis V, Bahuguna S and Soldatos D 2004 On the thermomechanical modeling of shape memory alloys *Int. J. Non-Linear Mech.* **39** 709

[10] Abeyarante R and Knowles J K 1991 Kinetic relations and the propagation of phase boundaries in solids *Arch. Ration. Mech. Anal.* **114** 119–54

[11] Truskinovsky L 1993 *Kinks versus Shocks, in Shock Induced Transitions and Phase Structures in General Media* (Berlin: Springer)

[12] Shaw J 2002 A thermomechanical model for a 1-D shape memory alloy wire with propagating instabilities *Int. J. Solids Struct.* **39** 1275

[13] Sun Q P and Hwang K C 1993 Micromechanics modelling for the constitutive behavior of polycrystalline shape memory alloys—I *J. Mech. Phys. Solids* **41** 1–17

[14] Gao X and Brinson C 2002 A simplified multivariant SMA model based on invariant plane nature of martensitic transformation *J. Intell. Mater. Syst. Struct.* **13** 795–810

[15] Tanaka K and Nagaki S 1982 A thermomechanical description of materials with internal variables in the process of phase transformation *Ing.-Arch.* **51** 287–99

[16] Liang C 1990 The constitutive modeling of shape memory alloys *PhD Thesis* Virginia Tech, Blacksburg, VA

[17] Tanaka K 1986 A thermomechanical sketch of shape memory effect: one-dimensional tensile behavior *Res. Mech., Int. J. Struct. Mach. Mater. Sci.* **18** 251–63

[18] Liang C and Rogers C A 1990 One-dimensional thermomechanical constitutive relations for shape memory materials *J. Intell. Mater. Syst. Struct.* **1** 207–34

[19] Bekker A and Brinson L C 1997 Temperature-induced phase transformation in a shape memory alloy: phase diagram kinetics approach *J. Mech. Phys. Solids* **45** 949–88

[20] Bekker A and Brinson L C 1998 Phase diagram based description of the hysteresis behavior of shape memory alloys *Acta Mater.* **46** 3649–65

[21] Waram T 1993 *Actuator Design Using Shape Memory Alloys* 2nd edn (Ontario, Canada: TC Waram)

[22] Elahinia M H and Ashrafiuon H 2002 Nonlinear control of a shape memory alloy actuated manipulator *ASME J. Vib. Acoust.* **124** 566–75

[23] Elahinia M H, Seigler T M, Leo D J and Ahmadian M 2004 Nonlinear stress-based control of a rotary SMA-actuated manipulator *J. Intell. Mater. Syst. Struct.* **15** 495–508

[24] Bhattacharyya A, Lagoudas D C A, Wang Y and Kinra V K 1995 On the role of thermoelectric heat transfer in the design of sma actuators: theoretical modeling and experiments *Smart Mater. Struct.* **4** 252–63

[25] Bhattacharyya A, Sweeney L and Faulkner M G 2002 Experimental characterization of free convection during thermal phase transformation in shape memory alloy wires *Smart Mater. Struct.* **11** 411–22

[26] Potapov P L and da Silva E P 2000 Time response of shape memory alloy actuators *J. Intell. Mater. Syst. Struct.* **11** 125–34

[27] Çengel Y A 1998 *Heat Transfer: A Practical Approach* 2nd edn (Princeton, NJ: McGraw-Hill)